On the existence and strength of stable membrane protrusions

2013 New J. Phys. 15 015021

(http://iopscience.iop.org/1367-2630/15/1/015021)

New Journal of Physics
The open access journal for physics

On the existence and strength of stable membrane protrusions

Juliane Zimmermann and Martin Falcke[1]
Mathematical Cell Physiology, Max-Delbrück-Center for Molecular Medicine, Robert-Rössle-Straße 10, D-13092 Berlin, Germany
E-mail: martin.falcke@mdc-berlin.de

New Journal of Physics **15** (2013) 015021 (25pp)
Received 10 September 2012
Published 28 January 2013
Online at http://www.njp.org/
doi:10.1088/1367-2630/15/1/015021

Abstract. We present a mathematical model for the protrusion of lamellipodia in motile cells. The model lamellipodium consists of a viscoelastic actin gel in the bulk and a dynamic boundary layer of newly polymerized filaments at the leading edge called the semiflexible region (SR). The density of filaments in the SR can increase due to nucleation of new filaments and decrease due to capping and severing of existing filaments. Following on from previous publications, we present important approximations that make the model feasible and accessible to fast computational analysis. It reveals that there are three qualitatively different parameter regimes: a stable, stationarily protruding lamellipodium; a stable lamellipodium showing oscillatory motion of the leading edge; and zero filament density and no stable lamellipodium. Hence, the model defines criteria for the existence of lamellipodia and the ability of cells to move effectively, and we discuss which parameter changes can induce transitions between the different states. Furthermore, stable lamellipodia have to be able to exert and withstand substantial forces. We can fit the experimentally measured dynamic force–velocity relation that describes how cells can adapt to increasing external forces when encountering an obstacle in their environment during motion. Moreover, we predict a different stationary force–velocity relation that should apply if cells experience a constant force, e.g. exerted by the surrounding tissue.

[1] Author to whom any correspondence should be addressed.

Contents

1. Introduction

Cell motility plays a key role in neural development, wound healing, the immune response [1] and in metastasis of cancer cells [2]. Understanding the mechanisms of cell motility is a prerequisite for finding a means of inhibiting cancer spread [3, 4].

Many motile cells form a lamellipodium in the direction of motion, which is a flat protrusion supported by an actin filament network. The force of protrusion in the lamellipodium is believed to arise from the polymerization of actin [5, 6]. Actin polymers are found in bundles in the interior of the lamellipodium, where myosin motor molecules can move along them to create contractions. Toward the leading edge, actin forms a polar network with the fast polymerizing barbed ends directed toward the membrane. At the opposite pointed ends, filaments depolymerize, actin monomers are recycled and diffuse to the front, where they are consumed by the growing tips [7]. This process is called treadmilling and is regulated by several proteins [8–13]. Arp2/3 (actin-related protein 2/3) binds to an existing actin filament and nucleates a new branch. Arp2/3 is activated by nucleation promoting factors, such as the membrane-associated WASP, N-WASP or WAVE. Activation is restricted usually to the leading edge membrane. Capping proteins bind to the barbed end of a filament and prevent polymerization and depolymerization there. Cofilin binds to filaments, enhances depolymerization and severs them. Different kinds of cross-linking proteins connect filaments and provide mechanical stability to the network. Other proteins are believed to bind actin polymers to the membrane [14].

The protrusions of motile cells consist of the posterior lamellum with highly cross-linked and bundled actin filaments and the anterior lamellipodium with a network of individual filaments polymerizing against the leading edge membrane [15–20]. While earlier studies suggested the lamellipodial actin network to be highly cross-linked very close to the leading edge membrane already due to branching of filaments by the Arp2/3 complex [21, 22], more

recent studies showed that the branch point density in the lamellipodium may be rather low and the lamellipodium-like structures may extend several hundreds of nanometers into the cell [23–26]. That view is also supported by the mechanical properties of the anterior region, which is as soft as *weakly* cross-linked actin networks [6, 27–30]. The studies also differ in their results on filament length. While some conclude that filaments in the lamellipodium have a length of a few hundreds of nanometers [21, 22], others find the length in the micrometer range [19, 23, 24, 28, 31, 32].

The force balance at the surface of the object propelled by actin polymerization comprises forces driving and resisting the motion. Polymerizing actin filaments generate motion [11, 33]. The forces resisting it are only in part drag forces. They arise not so much from the fluid surrounding drops or beads as from friction with the actin network. Cell motion involves membrane motion relative to the substrate and to adhesion sites as well as fluid transport. That also causes forces resisting motion which increase with the velocity. A major contribution to the resisting forces comes from filaments bound to the object surface and pulling on it. That has been shown for beads [5] and oil drops [34] directly. The presence of a large variety of actin binding membrane proteins or proteins linking F-actin to membrane proteins in the leading edge of lamellipodia (reviewed in [14]) strongly suggests that filaments attach also to the membrane and hold it back. Additionally, membrane tension resists protrusion in spreading and motile cells [35–38].

Here, we first present an extension of a model used in a variety of previous modeling studies and then apply the model to questions relevant for cell function. We extend the model to include total filament number dynamics due to capping, nucleation and severing. Changes in filament number were not important for the quantitative modeling of the dynamic force–velocity experiments lasting about 10 s only [30] or morphodynamics on the time scale of a few tens of seconds [39]. But they are so for the stationary response of cells to forces, since the filament number can adjust if force is applied for a long time [40].

The model without capping and nucleation describes the free filament length changes in the semiflexible region (SR). Because shortening of the free filament length by cross-linking is compensated for by filament elongation due to polymerization, all filaments quickly assume the same free length [41]. Based on a monodisperse approximation, we solve equations for the mean filament length. That monodisperse approximation cannot be applied to capped filaments, since they do not polymerize and their length depends on the time of capping. An exact approach requires the time-dependent solution of the partial differential equation for the length distribution dynamics of capped filaments [42]. That can be done analytically but only up to a remaining time integral, which renders the model very slow in simulations and rather inaccessible to analysis. Here, we present the methods and approximations leading in the end to a much simpler model formulation.

We apply the model to calculate the stationary force–velocity relation, but also show that it reproduces the dynamic one. The model enables us also to investigate conditions for protrusion existence. Both, the existence of stable protrusions and the stationary force–velocity relation are crucial for cell behavior in tissue. The existence of protrusions is a prerequisite for mesenchymal (lamellipodial) motion. Since the forces exerted by surrounding tissue on a cell act over a long time, the stationary force–velocity relation applies and not so much the dynamic one which has been measured *in vitro* [6, 29, 30].

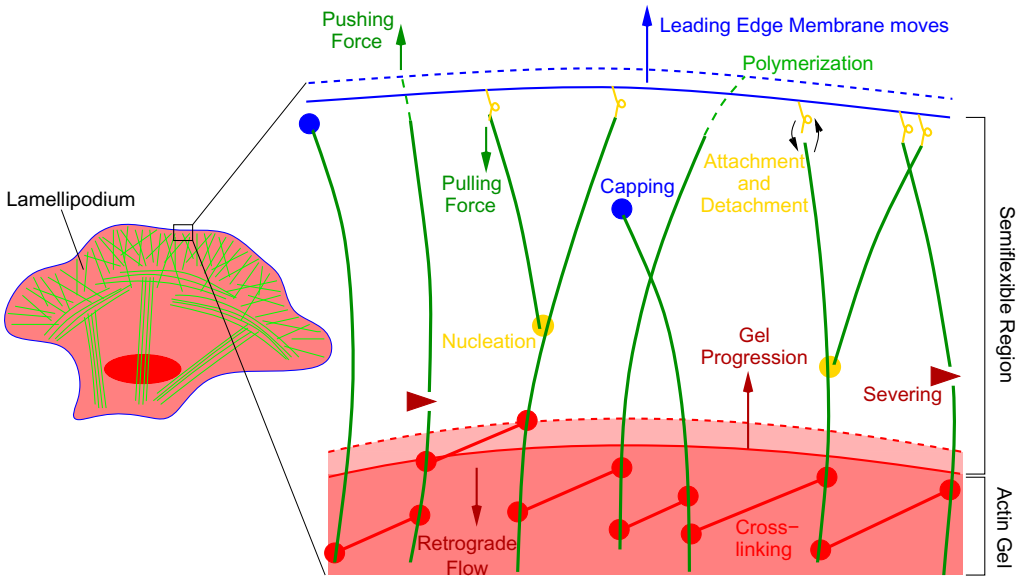

Figure 1. Schematic representation of the processes included in the model. The actin filaments (green) in the semiflexible region (SR) can fluctuate and bend. They exert forces on the leading edge membrane (blue line) and push it forward. They elongate by polymerization and shorten by attachment of cross-linkers (red dumbbells), which advances the gel boundary (red line) defined by a critical concentration of bound cross-linkers. Retrograde flow in the actin gel counteracts forward motion of the gel boundary. Filaments can also attach to the leading edge membrane and exert a pulling force. New filaments are nucleated from attached filaments. Filaments can get capped or severed and vanish into the gel afterwards.

2. The model

2.1. Modeling concept

The model includes the dense cross-linked actin gel in the bulk and the SR at the leading edge of the lamellipodium (see figure 1). The boundary between the gel and the SR is defined by a critical concentration of cross-linkers bound to the actin filaments. The density of filaments in the SR changes by nucleation of new filaments and capping and severing of existing filaments. Filaments in the SR can attach to the leading edge membrane via linker proteins. Attached filaments can not only push, but also pull the membrane. The leading edge dynamics is determined by the balance of filament forces and forces resisting motion.

2.2. Filament forces

Semiflexible actin filaments are subject to Brownian motion at the length scale of cells since their persistence length l_p is in the same range. Filaments of contour length l grafted at one end exert an entropic force on an obstacle at distance z. The force has been calculated in [43] as

$$F_d(z, l, l_p) = F_{crit}\tilde{F}(\tilde{\eta}), \tag{1}$$

with the scaling variable

$$\tilde{\eta} = \frac{l - z}{l_\parallel}, \quad l_\parallel = \frac{l^2}{l_\mathrm{p}}, \tag{2}$$

and

$$F_\mathrm{crit} = \frac{\pi^2}{4}\frac{k_\mathrm{B}T}{l_\parallel} \tag{3}$$

is the critical force for the Euler buckling instability. In [43], it is shown that for small compression $\tilde{\eta} \lesssim 0.2$, the scaling function of the entropic force can well be approximated as

$$\tilde{F}^{<}(\tilde{\eta}) = \frac{4\exp(-\frac{1}{4\tilde{\eta}})}{\pi^{5/2}\tilde{\eta}^{3/2}\left[1 - 2\,\mathrm{erfc}\left(1/(2\sqrt{\tilde{\eta}})\right)\right]}. \tag{4}$$

For $\tilde{\eta} \gtrsim 0.2$ the calculation yields

$$\tilde{F}^{>}(\tilde{\eta}) = \frac{1 - 3\exp(-2\pi^2\tilde{\eta})}{1 - \frac{1}{3}\exp(-2\pi^2\tilde{\eta})}. \tag{5}$$

The situation is different for attached filaments, since the tip of the filament is always positioned at the membrane and cannot fluctuate. The proteins linking the filaments to the membrane are assumed to behave like elastic springs. We distinguish three different regimes for the force F_a exerted by the serial arrangement of polymer and linker, depending on the relation between the depth of the semi-flexible region z, the equilibrium end-to-end distance $R_\parallel = l(1 - l/2l_\mathrm{p})$ and the contour length l [44]:

$$F_\mathrm{a}(l, z) = \begin{cases} -k_\parallel(z - R_\parallel), \ z \leqslant R_\parallel, & \text{(i)} \\ -k_\mathrm{eff}(z - R_\parallel), \ R_\parallel < z < l, & \text{(ii)} \\ -k_l(z - l) - k_\mathrm{eff}(l - R_\parallel), \ z \geqslant l. & \text{(iii)} \end{cases} \tag{6}$$

The three cases correspond to: (i) a compressed filament pushes against the membrane; (ii) filament and linker pull the membrane while being stretched together; and (iii) a filament is fully stretched but the linker continues to pull the membrane by being stretched further. Here, $k_\parallel$, k_l and k_eff are the linear elastic coefficients of polymer, linker and serial polymer–linker arrangement, respectively. For $k_\parallel$ we use the linear response coefficient of a worm-like chain grafted at both ends $k_\parallel = 6k_\mathrm{B}Tl_\mathrm{p}^2/l^4$ [45, 46].

2.3. Rates

Detached filaments attach to the membrane with a constant rate k_a. The detachment rate of attached filaments is force dependent since a pulling force facilitates detachment. It can be expressed as

$$k_\mathrm{d} = k_\mathrm{d}^0 \exp(-dF_\mathrm{a}/k_\mathrm{B}T), \tag{7}$$

with the force-free detachment rate k_d^0. The length increment d added by an actin monomer to the filament is 2.7 nm.

Detached filaments can polymerize and grow. The velocity of polymerization is force dependent because the probability that the filament fluctuates away from the membrane and

a gap sufficiently large for insertion of an actin monomer appears decreases with increasing the force [47]. The polymerization velocity reads

$$v_\mathrm{p} = v_\mathrm{p}^\mathrm{max} \exp(-d F_\mathrm{d}/k_\mathrm{B}T). \tag{8}$$

$v_\mathrm{p}^\mathrm{max}$ is the maximum polymerization velocity depending on the actin monomer concentration.

The rate of filament shortening is contour length dependent. The filaments are shortened by the attachment of cross-linker molecules and incorporation of filament length into the actin gel. The cross-linking velocity is length dependent, since the cross-linker binding probability increases with filament length. It is unlikely that very short filaments get cross-linked. Free cross-linker molecules bind to filaments near the leading edge. Retrograde flow of the actin network transports them as bound molecules to the rear, where they dissociate and diffuse back to the front. Solving the corresponding reaction–diffusion equation, we have shown [48] that the cross-linking velocity can be expressed as

$$v_\mathrm{g}(l, n) = \hat{v}_\mathrm{g}^\mathrm{max} n \tanh(nl/\bar{l}). \tag{9}$$

It is proportional to the filament density n, because denser filament packing allows cross-linkers to span the inter-filament distance more easily. The characteristic length $\bar{l}$ and the maximum cross-linking rate $\hat{v}_\mathrm{g}^\mathrm{max}$ are parameters. In the rate of filament shortening $\tilde{v}_\mathrm{g}(l, z, n) = \max(1, v_\mathrm{g} l/z)$, the additional factor l/z accounts for the fact that a larger portion of filament length is incorporated into the gel during cross-linking when filaments are bent.

Detached filaments may get capped. The binding rate of capping proteins is force dependent, similar to the attachment of actin monomers to the filament barbed ends during polymerization. We find an Arrhenius factor in the capping rate

$$k_\mathrm{c} = k_\mathrm{c}^\mathrm{max} \exp(-d F_\mathrm{d}/k_\mathrm{B}T). \tag{10}$$

New filament branches are nucleated by Arp2/3 off attached filaments with a nucleation rate k_n. We assume nucleation from *attached* filaments since activation of the Arp2/3 complex by nucleation-promoting factors involves membrane binding. New filaments enter the force balance and thus the SR dynamics when they reach the support by the actin gel. Since the branching point vanishes into the gel quickly, newly nucleated filaments have the same length as the mother filament in our model. The total number n of filaments is undefined without a feedback to the nucleation process [42]. Such a feedback could be caused by a limited number of Arp2/3 proteins. The effective nucleation rate reads

$$k_\mathrm{n} = k_\mathrm{n}^0 - k_\mathrm{n}^N n. \tag{11}$$

The rates k_n^0 and k_n^N are constants.

We also want to include the disassembly of actin filaments by ADF/cofilin into our model. ADF/cofilin binds to ADP-actin within filaments and promotes its dissociation by severing and depolymerization of filaments [33]. We hypothesize that filaments to which cofilin is bound vanish from the SR because they cannot exert a force any longer once they are severed. Actin filaments bind ATP-actin monomers at their plus ends and quickly hydrolyze ATP to ADP-Pi but it takes longer to lose the y-phosphate. Cofilin only binds to ADP-actin when y-phosphate has dissociated [49, 50]. We can describe the dissociation by an exponential decay. The half lifetime for y-phosphate dissociation within the filament is 6 min [33]. We neglect that y-phosphate dissociation is probably accelerated by cofilin. The probability of cofilin binding is proportional to the probability of finding an ADP-actin monomer at a given site x from the tip of the filament:

$$p_\mathrm{ADP} = 1 - \mathrm{e}^{-t \ln(2)/T_{1/2}} = 1 - \mathrm{e}^{-x \ln(2)/(v_\mathrm{p}^\mathrm{max} T_{1/2})}. \tag{12}$$

We assume that the polymerization velocity is constant v_p^{max}. The probability of filament severing is found by integrating over the whole filament length

$$p_{sev} = \int_0^l 1 - e^{-x \ln(2)/(v_p^{max} T_{1/2})} dx = l + \frac{v_p^{max} T_{1/2}}{\ln(2)} \left(e^{-\frac{\ln(2) l}{v_p^{max} T_{1/2}}} - 1 \right). \tag{13}$$

That leads to l-dependent terms in the dynamics of the number of attached and detached filaments.

2.4. Gel velocity and retrograde flow

We have calculated the retrograde flow velocity in the actin gel [48] using the theory of the active polar gel by Kruse *et al* [51, 52]. It depends linearly on the force acting on the leading edge membrane. Solving the gel equations leads to the expressions for the coefficients of this linear equation as a function of the gel parameters. We obtain for the gel velocity

$$\begin{aligned} u &\approx v_{link} - \frac{\mu L}{4\eta} g_1 + \frac{f_0}{L\xi} g_2, \\ g_1 &= \frac{1}{2.0 + 0.12 \frac{\xi L^2}{4\eta h_0}}, \\ g_2 &= \left(1.0 + 0.92 \frac{\xi L^2}{h_0 4\eta} \right)^{1/2} \left(1.0 + 0.03 \frac{\mu L}{4\eta v_{link}} \right). \end{aligned} \tag{14}$$

Here, v_{link} is the cross-linking velocity, hence the velocity at which the actin gel is produced. The gel boundary does not move forward with the velocity of cross-linking since there is a backwards-directed retrograde flow in the actin gel. The term proportional to g_1 expresses the retrograde flow arising from contractile stress μ in the actin gel. Contractions may be caused by myosin motors or actin depolymerization [53]. $L = 10\,\mu$m is the width of the gel part of the lamellipodium and η is the viscosity of the actin gel. The g_2-term describes a retrograde flow due to filaments in the SR pushing the gel backwards. The total force that they exert on the gel boundary is denoted by f_0. Adhesions between the gel and the substrate are described by the friction coefficient ξ. h_0 is the height of the lamellipodium at the boundary between the gel and the SR. We have fit g_1, g_2 for $0 \leqslant \frac{\xi L^2}{4\eta h_0} \leqslant 50$. Equations (14) are valid on the condition that $\frac{\mu L}{4\eta v_{link}} < 1$.

2.5. Dynamic equations

The processes considered so far determine the length distribution of attached $N_a(l, t)$, detached $N_d(l, t)$ and capped filaments $N_c(l, t)$ in the SR. Their dynamics are described by the following linear equations (see also [42]):

$$\begin{aligned} \frac{\partial}{\partial t} N_d(l,t) = {} & \frac{\partial}{\partial l}((\tilde{v}_g - v_p) N_d(l,t)) + k_d N_a(l,t) - k_a N_d(l,t) - k_c N_d(l,t) \\ & - k_{sev} N_d(l,t) \left[l + \frac{v_p^{max} T_{1/2}}{\ln(2)} \left(e^{-\frac{l \ln(2)}{v_p^{max} T_{1/2}}} - 1 \right) \right], \end{aligned} \tag{15}$$

$$\frac{\partial}{\partial t}N_{\mathrm{a}}(l,t)=\frac{\partial}{\partial l}(\tilde{v}_{\mathrm{g}}N_{\mathrm{a}}(l,t))-k_{\mathrm{d}}N_{\mathrm{a}}(l,t)+k_{\mathrm{a}}N_{\mathrm{d}}(l,t)+k_{\mathrm{n}}N_{\mathrm{a}}(l,t)$$
$$-k_{\mathrm{sev}}N_{\mathrm{a}}(l,t)\left[l+\frac{v_{\mathrm{p}}^{\max}T_{1/2}}{\ln(2)}\left(\mathrm{e}^{-\frac{l\ln(2)}{v_{\mathrm{p}}^{\max}T_{1/2}}}-1\right)\right], \tag{16}$$

$$\frac{\partial}{\partial t}N_{\mathrm{c}}(l,t)=\frac{\partial}{\partial l}(\tilde{v}_{\mathrm{g}}N_{\mathrm{c}}(l,t))+k_{\mathrm{c}}N_{\mathrm{d}}(l,t). \tag{17}$$

k_{sev} is the binding rate of cofilin.

As shown in [41, 42], a δ-function-ansatz for $N_{\mathrm{d}}(l)$ and $N_{\mathrm{a}}(l)$ used in equations (15) and (16) leads to ordinary differential equations for the total density of attached and detached filaments n_{a} and n_{d} and for their mean lengths l_{a} and l_{d}:

$$\dot{n}_{\mathrm{d}}=k_{\mathrm{d}}n_{\mathrm{a}}-(k_{\mathrm{a}}+k_{\mathrm{c}})n_{\mathrm{d}}-k_{\mathrm{sev}}n_{\mathrm{d}}\left[l_{\mathrm{d}}+\frac{v_{\mathrm{p}}^{\max}T_{1/2}}{\ln(2)}\left(\mathrm{e}^{-\frac{l_{\mathrm{d}}\ln(2)}{v_{\mathrm{p}}^{\max}T_{1/2}}}-1\right)\right], \tag{18}$$

$$\dot{n}_{\mathrm{a}}=k_{\mathrm{a}}n_{\mathrm{d}}-(k_{\mathrm{d}}-k_{\mathrm{n}})n_{\mathrm{a}}-k_{\mathrm{sev}}n_{\mathrm{a}}\left[l_{\mathrm{a}}+\frac{v_{\mathrm{p}}^{\max}T_{1/2}}{\ln(2)2}\left(\mathrm{e}^{-\frac{l_{\mathrm{a}}\ln(2)}{v_{\mathrm{p}}^{\max}T_{1/2}}}-1\right)\right], \tag{19}$$

$$\dot{l}_{\mathrm{d}}=-(\tilde{v}_{\mathrm{g}}(l_{\mathrm{d}},z,n)-v_{\mathrm{p}}(l_{\mathrm{d}},z))+k_{\mathrm{d}}(l_{\mathrm{a}},z)\frac{n_{\mathrm{a}}(t)}{n_{\mathrm{d}}(t)}(l_{\mathrm{a}}(t)-l_{\mathrm{d}}(t)), \tag{20}$$

$$\dot{l}_{\mathrm{a}}=-\tilde{v}_{\mathrm{g}}(l_{\mathrm{a}},z,n)+k_{\mathrm{a}}\frac{n_{\mathrm{d}}(t)}{n_{\mathrm{a}}(t)}(l_{\mathrm{d}}(t)-l_{\mathrm{a}}(t)). \tag{21}$$

The dynamics of the SR width reads

$$\dot{z}=\frac{1}{\kappa}(f_0-f_{\mathrm{ext}})-u(v_{\mathrm{link}},-f_0), \tag{22}$$

with the total filament force

$$f_0=(F_{\mathrm{d}}(l_{\mathrm{d}},z)n_{\mathrm{d}}(t)+F_{\mathrm{a}}(l_{\mathrm{a}},z)n_{\mathrm{a}}(t)+f_{\mathrm{c}}(n_{\mathrm{d}},l_{\mathrm{d}},z,n)). \tag{23}$$

We have also included a constant external force f_{ext} that acts on the leading edge. Expression (14) is used for the gel boundary velocity u. The total force of capped filaments f_{c}, the average cross-linking rate v_{link} and the total filament density n will be calculated below.

2.6. Length distribution of capped filaments

The monodisperse approximation is not valid for the distribution of capped filaments $N_{\mathrm{c}}(l,t)$. That renders the calculation of $N_{\mathrm{c}}(l,t)$ much more complicated than it was for the other densities. However, we need $N_{\mathrm{c}}(l,t)$ for its contributions f_{c} to the force, n_{c} to the total number of filaments and $v_{\mathrm{g}}^{\mathrm{c}}$ to the average cross-linking velocity v_{link} (see equation (42)).

Equation (17) is solved using the method of characteristics. Here, we assume that filaments are long when they get capped. We neglect the length dependence of v_{g} and only account for $\tilde{v}_{\mathrm{g}}=\max(1,l/z)\hat{v}_{\mathrm{g}}^{\max}n$. As before, we write $v_{\mathrm{g}}^{\max}(n)=\hat{v}_{\mathrm{g}}^{\max}n$. Furthermore, we are only interested in $N_{\mathrm{c}}(l,t)$ for $z\leqslant l\leqslant l_{\mathrm{d}}$, since for $l<z$, capped filaments exert no force.

Hence, $\tilde{v}_g = \frac{l}{z} v_g^{max}$. Using the monodisperse approximation for the detached filaments $N_d(l,t) = n_d(t)\delta(l - l_d(t))$, equation (17) reads

$$\frac{\partial}{\partial t} N_c = \frac{v_g^{max}}{z} N_c + \frac{l}{z} v_g^{max} \frac{\partial}{\partial l} N_c + k_c(l_d) n_d(t) \delta(l - l_d). \tag{24}$$

With

$$\frac{dN}{ds} = \frac{\partial N}{\partial t}\frac{dt}{ds} + \frac{\partial N}{\partial l}\frac{dl}{ds}, \tag{25}$$

we can identify the characteristics

$$\frac{dt}{ds} = 1\,, \quad \frac{dl}{ds} = -v_g^{max}\frac{l}{z} \tag{26}$$

and

$$\frac{dN_c}{ds} = \frac{v_g^{max}}{z} N_c + k_c(l_d) n_d(t) \delta(l - l_d). \tag{27}$$

The first equation (the first of equations (26)) gives $s = t$ and therefore we obtain

$$\frac{dl}{dt} = -\frac{v_g^{max}}{z} l \tag{28}$$

with the solution (obtained by separation of variables)

$$l(t) = l(t^*) \exp\left(- \int_{t^*}^{t} \frac{v_g^{max}(t')}{z(t')} dt' \right). \tag{29}$$

The time point of capping is denoted by t^*. Solving

$$\frac{dN_c}{dt} = \frac{v_g^{max}}{z} N_c + k_c(l_d) n_d(t) \delta(l - l_d) \tag{30}$$

requires a little more effort. The general solution of the inhomogeneous equation equals the sum of the solution of the homogeneous equation and a special solution of the inhomogeneous equation. The solution of the homogeneous equation reads

$$N_c^h = C \exp\left(\int_{t^*}^{t} \frac{v_g^{max}}{z} dt' \right). \tag{31}$$

The special solution of the inhomogeneous equation is found by the variation of constants:

$$\begin{aligned} N_c^{sp} &= \left[\int_{t^*}^{t} dt' k_c(l_d(t')) n_d(t') \delta(l(t') - l_d(t') \exp\left(- \int_{t^*}^{t'} \frac{v_g^{max}}{z} dt'' \right) \right] \exp\left(\int_{t^*}^{t} \frac{v_g^{max}}{z} dt' \right) \\ &= \int_{t^*}^{t} dt' k_c(l_d(t')) n_d(t') \delta(l(t') - l_d(t') \exp\left(\int_{t'}^{t} \frac{v_g^{max}}{z} dt'' \right) \\ &= \frac{k_c(l_d(t^*)) n_d(t^*)}{|\frac{d}{dt'}(l(t') - l_d(t'))|_{t'=t^*}} \exp\left(\int_{t^*}^{t} \frac{v_g^{max}}{z} dt'' \right). \end{aligned}$$

In the last line, we have used $\delta(g(x)) = \sum_{i=1}^{n} \frac{\delta(x - x_i)}{|g'(x_i)|}$, where x_i are the roots of $g(x)$. Note that $l(t^*) = l_d(t^*)$ at the time of capping t^*. Equation (29) yields

$$\exp\left(\int_{t^*}^{t} \frac{v_g^{max}}{z} dt'' \right) = \frac{l_d(t^*)}{l(t)}. \tag{32}$$

We find that

$$\frac{\mathrm{d}}{\mathrm{d}t}l(t)|_{t=t^*} = -\frac{v_\mathrm{g}^{\max}(t^*)}{z(t^*)}l_\mathrm{d}(t^*)$$

using (29). Furthermore,

$$\frac{\mathrm{d}}{\mathrm{d}t}l_\mathrm{d}(t)|_{t=t^*} = -\frac{v_\mathrm{g}^{\max}(t^*)}{z(t^*)}l_\mathrm{d}(t^*) + v_\mathrm{p}(l_\mathrm{d}(t^*)) + k_\mathrm{d}(l_\mathrm{a}(t^*))\frac{n_\mathrm{a}(t^*)}{n_\mathrm{d}(t^*)}(l_\mathrm{a}(t^*) - l_\mathrm{d}(t^*)).$$

Hence,

$$N_\mathrm{c}^\mathrm{sp}(t, t^*) = \frac{k_\mathrm{c}(l_\mathrm{d}(t^*))n_\mathrm{d}(t^*)}{v_\mathrm{p}(l_\mathrm{d}(t^*)) + k_\mathrm{d}(l_\mathrm{a}(t^*))\frac{n_\mathrm{a}}{n_\mathrm{d}}(t^*)(l_\mathrm{a}(t^*) - l_\mathrm{d}(t^*))}\frac{l_\mathrm{d}(t^*)}{l(t)} \tag{33}$$

for $k_\mathrm{d}(l_\mathrm{a}(t^*))\frac{n_\mathrm{a}}{n_\mathrm{d}}(t^*)(l_\mathrm{a}(t^*) - l_\mathrm{d}(t^*)) > -v_\mathrm{p}(l_\mathrm{d}(t^*))$. To find the length distribution of capped filaments, for every length l, t^* has to be calculated by solving $l = l_\mathrm{d}(t^*)$. The number of capped polymers is determined by the number of detached polymers and the capping rate at the time of capping.

2.7. The total number, force and cross-linking rate of capped filaments

For calculating the total number, force and cross-linking rate, we need

$$\begin{aligned}
\frac{\partial l}{\partial t^*} &= \frac{\partial}{\partial t^*}\left[l_\mathrm{d}(t^*)\exp\left(-\int_{t^*}^{t}\frac{v_\mathrm{g}^{\max}(t')}{z(t')}\mathrm{d}t'\right)\right] \\
&= \left[\dot{l}_\mathrm{d}(t^*) - \left(-\frac{v_\mathrm{g}^{\max}}{z}(t^*)\right)l_\mathrm{d}(t^*)\right]\exp\left(-\int_{t^*}^{t}\frac{v_\mathrm{g}^{\max}(t')}{z(t')}\mathrm{d}t'\right) \\
&= \left[-\frac{v_\mathrm{g}^{\max}}{z}l_\mathrm{d}(t^*) + v_\mathrm{p}(t^*) + k_\mathrm{d}\frac{n_\mathrm{a}}{n_\mathrm{d}}(l_\mathrm{a} - l_\mathrm{d})(t^*) + \frac{v_\mathrm{g}^{\max}}{z}l_\mathrm{d}(t^*)\right]\exp\left(-\int_{t^*}^{t}\frac{v_\mathrm{g}^{\max}}{z}\mathrm{d}t'\right) \\
&= \left[v_\mathrm{p}\left(l_\mathrm{d}(t^*)\right) + k_\mathrm{d}\left(l_\mathrm{a}(t^*)\right)\frac{n_\mathrm{a}}{n_\mathrm{d}}(t^*)\left(l_\mathrm{a}(t^*) - l_\mathrm{d}(t^*)\right)\right]\exp\left(-\int_{t^*}^{t}\frac{v_\mathrm{g}^{\max}(t')}{z(t')}\mathrm{d}t'\right).
\end{aligned}$$

The total density of capped filaments with $z \leqslant l \leqslant l_\mathrm{d}$ is then given by

$$n_\mathrm{c} = \int_{z(t)}^{l_\mathrm{d}(t)}\mathrm{d}l\, N_\mathrm{c}(l, t) = \int_{t_z^*}^{t}\mathrm{d}t^*\frac{\partial l}{\partial t^*}N_\mathrm{c}(t^*, t) = \int_{t_z^*}^{t}\mathrm{d}t^* k_\mathrm{c}\left(l_\mathrm{d}(t^*), z(t^*)\right)n_\mathrm{d}(t^*). \tag{34}$$

The lower integral boundary is $z(t)$ since shorter filaments do not exert any force and are therefore not considered in the model. The time of capping of filaments with length z at time t corresponds to t_z^*. We again use equation (29)

$$z(t) = l_\mathrm{d}(t_z^*)\exp\left(-\int_{t_z^*}^{t}\frac{v_\mathrm{g}^{\max}(t')}{z(t')}\mathrm{d}t'\right) \tag{35}$$

and apply a root finding algorithm to determine t_z^*. The total number of all filaments is given by $n = n_\mathrm{c} + n_\mathrm{a} + n_\mathrm{d}$.

Along these lines, we can also calculate the total force of capped filaments

$$f_\mathrm{c} = \int_{z(t)}^{l_\mathrm{d}(t)}\mathrm{d}l\, N_\mathrm{c}(l, t)F_\mathrm{d}(l, z) = \int_{t_z^*}^{t}\mathrm{d}t^* k_\mathrm{c}\left(l_\mathrm{d}(t^*), z(t^*)\right)n_\mathrm{d}(t^*)F_\mathrm{d}\left(l(t^*), z(t)\right). \tag{36}$$

Note that we have to calculate $l(t^*)$ according to expression (29) for every t^*. The average cross-linking rate yields

$$v_g^c = \frac{1}{n}\int_{z(t)}^{l_d(t)} \mathrm{d}l\, N_c(l,t) v_g(l,n) = \frac{1}{n}\int_{t_z^*}^{t} \mathrm{d}t^* k_c\left(l_d(t^*), z(t^*)\right) n_d(t^*) v_g\left(l(t^*), n(t)\right). \tag{37}$$

The total number of filaments (attached, detached and capped) n enters v_g^{max}, and n_c is therefore already required for determining t_z^* (equation (35)). The total number changes according to

$$\frac{\mathrm{d}n}{\mathrm{d}t} = k_n n_a(t) - v_g^{max}(t) N_c(l=z,t). \tag{38}$$

It increases by nucleation and decreases because capped filaments are eaten by the gel. We only consider capped filaments longer than z that exert a force in order to simplify the calculations. Capped filaments with length $l = z$ vanish at the rate of gel cross-linking from this filament population. Their number is determined by equation (33) for $l(t) = z(t)$.

2.8. Further approximations

To calculate t_z^* in every time step and integrate over F_d and v_g is computationally very demanding. We also want to avoid tracking the history of l_a, l_d, z, n_a, n_d and n. To simplify the calculation, we assume a stationary distribution $N_c(l)$. In the stationary case, we obtain

$$\begin{aligned} N_c(l) &= \int_{t^*}^{t} \mathrm{d}t' k_c(l_d(t')) n_d(t') \delta(l(t') - l_d(t') \exp\left(\int_{t'}^{t} \frac{v_g^{max}}{z}\mathrm{d}t''\right) \\ &= -\int_{l_d}^{l} \mathrm{d}l' \frac{z}{v_g^{max} l'} k_c n_d \delta(l' - l_d)\frac{l'}{l} = \frac{z k_c n_d}{l v_g^{max}}. \end{aligned} \tag{39}$$

We have changed the integration variable according to equation (28).

The total density of capped filaments that exert a force (i.e. with length $z < l < l_d$) reads

$$n_c = \int_z^{l_d} \mathrm{d}l\, N_c(l) = \frac{z k_c n_d}{v_g^{max}} \ln\left(\frac{l_d}{z}\right). \tag{40}$$

With $v_g^{max} = \hat{v}_g^{max}(n_a + n_d + n_c)$, we obtain

$$n_c = -\frac{n_a + n_d}{2} + \sqrt{\left(\frac{n_a + n_d}{2.0}\right)^2 + \ln\left(\frac{l_d}{z}\right)\frac{k_c n_d z}{\hat{v}_g^{max}}}. \tag{41}$$

To calculate the average cross-linking rate,

$$v_{link} = \frac{1}{n}\left(n_a v_g(l_a) + n_d v_g(l_d) + v_g^c\right), \tag{42}$$

we again consider only capped filaments with $z \leqslant l \leqslant l_d$. We neglect the length dependence of v_g and set $v_g = v_g^{max}$ to obtain analytic expressions

$$v_g^c = \int_z^{l_d} v_g(l) N_c(l)\,\mathrm{d}l = z k_c n_d \int_z^{l_d} \frac{v_g(l)}{l v_g^{max}}\mathrm{d}l \approx z k_c n_d \int_z^{l_d} \frac{1}{l}\mathrm{d}l = z k_c n_d \ln\left(\frac{l_d}{z}\right). \tag{43}$$

The force of capped filaments is given by

$$f_c = \int_z^{l_d} \mathrm{d}l\, N_c(l) F_d(l,z) = \frac{k_c n_d z}{v_g^{max}} \int_z^{l_d} \frac{F_d}{l}\mathrm{d}l, \tag{44}$$

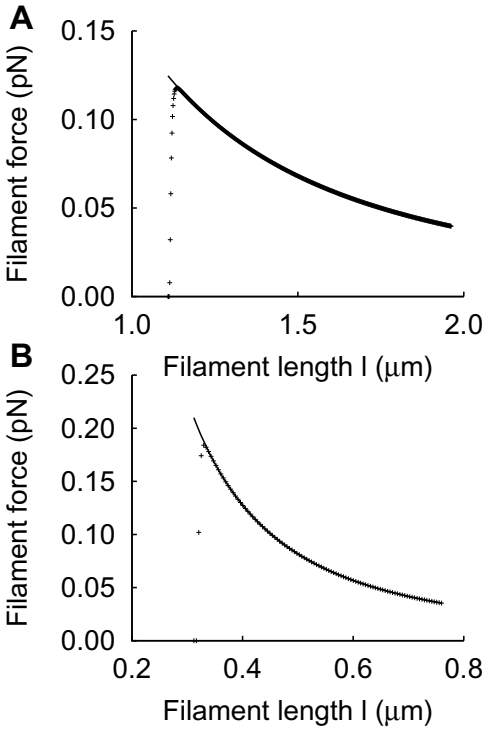

Figure 2. The force of capped filaments for $z \leqslant l \leqslant l_d$, which occurs in the integrand of equation (44), during a simulation of the system ($k_{sev} = 0$). (Crosses) The entropic force according to equation (1). (Solid line) Euler buckling force only (equation (3)) with the scaling function set to 1 as an approximation for the entropic force to obtain an analytic expression for the total force of capped filaments f_c (equation (45)). Only for lengths slightly larger than z the full entropic force differs from the Euler buckling force, so that the approximated f_c is slightly too large. However, the contribution of that part to the integral is very small and the approximation is good. (A) $l_p = 15\,\mu$m and (B) $l_p = 2\,\mu$m. Other parameters: $k_a = 0.833\,s^{-1}$, $k_d^0 = 1.67\,s^{-1}$, $k_n^0 = 2.0\,s^{-1}$, $k_n^N = 0.00167\,\mu m\,s^{-1}$, $k_c = 1.0\,s^{-1}$, $\hat{v}_g^{max} = 0.01\,\mu m^2\,min^{-1}$, $v_p^{max} = 50\,\mu m\,min^{-1}$, $\kappa = 0.833\,nN\,s\,\mu m^{-2}$, $\bar{l} = 10$, $\eta = 33.3\,nN\,s\,\mu m^{-2}$, $\xi = 10.0\,nN\,s\,\mu m^{-3}$, $\mu = 2.78\,pN\,s\,\mu m^{-2}$, $h_0 = 0.1\,\mu$m, $L = 10\,\mu$m.

with $F_d(l, z) = \frac{\pi^2}{4}\frac{k_B T l_p}{l^2}\tilde{F}(\tilde{\eta})$ (see equation (1)). The scaling function $\tilde{F}(\tilde{\eta})$ (equations (4) and (5)) cannot be integrated analytically. It increases monotonically to 1 with increasing the compression $\tilde{\eta}$ of the filament. When simulating the dynamical system we see that the $1/l^3$-dependence of the integrand of f_c dominates over the increasing part of $\tilde{F}$ (see figure 2). Therefore, we approximate F_d by the Euler buckling force F_{crit} and obtain

$$f_c = \frac{k_c n_d z}{v_g^{max}} \int_z^{l_d} \frac{\pi^2}{4}\frac{k_B T l_p}{l^3} dl = \frac{k_c n_d z}{v_g^{max}} \frac{\pi^2}{8} k_B T l_p \left(\frac{1}{z^2} - \frac{1}{l_d^2}\right). \tag{45}$$

In figure 3, we compare the solution of our time-dependent model with the solution of the model with the approximations introduced in this section.

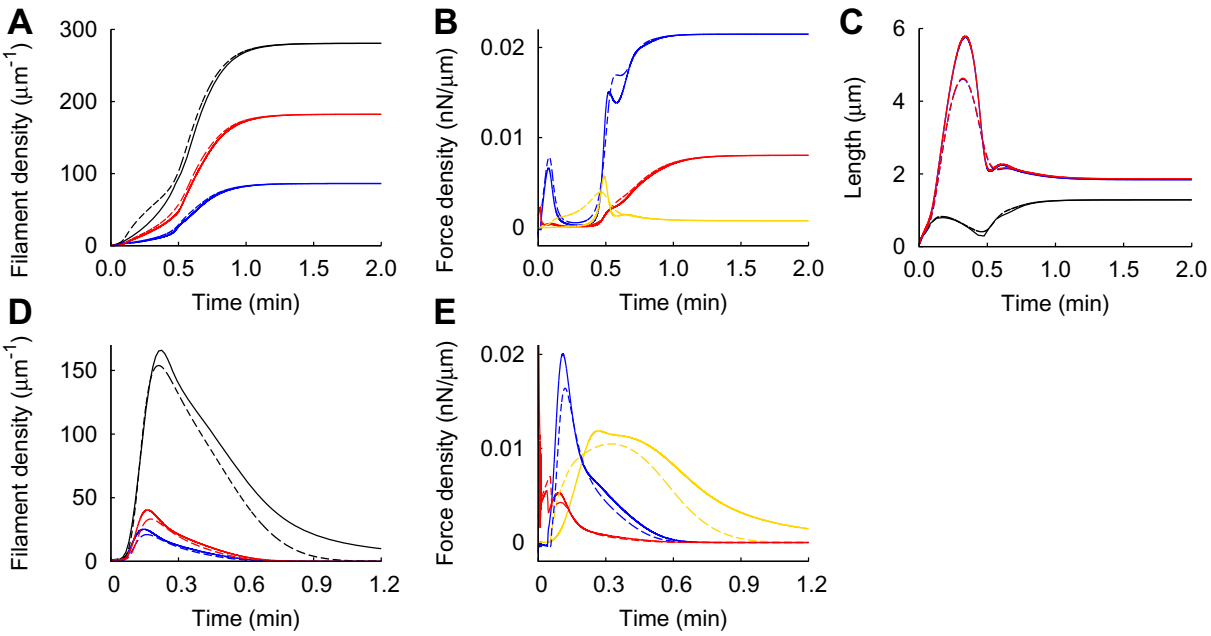

Figure 3. Comparison of the solution of the time-dependent model (solid lines) and the model with the approximations introduced in this section (dashed lines). (A)–(C) For the parameters from the fit of the force–velocity relation (table 1). (D), (E) For parameters in the regime with $n = 0$ as the stationary state: $k_n^0 = 2.0\,s^{-1}$, $k_c^{max} = 1.175\,s^{-1}$, all other parameters remain unchanged. Retrograde flow is set to zero. (A), (D) Density of attached filaments n_a (blue), detached filaments n_d (red) and the total filament density n (black). (B), (E) Force density of attached filaments f_a (blue), of detached filaments f_d (red) and capped filaments f_c (yellow). (C) Length of attached filaments l_a (blue), of detached filaments l_d (red) and SR depth z (black). Filament length is undetermined and increases steadily in the regime with $n = 0$.

3. Results

3.1. Existence of stable protrusions

Our model defines criteria for the existence of stable lamellipodia. In figure 4, we examine how the stationary filament density changes with some model parameters. The black areas indicate regions in the parameter space where $n = 0$ (no filaments in the SR) is the only stable fixed point. Since $n = 0$ means that there is no protrusion, the conditions for the existence of attractors with $n > 0$ (fixed points or limit cycles) describe the conditions for the existence of stable protrusions. Different sets of parameters in our model correspond to different cell types or different levels of expression or activation of signaling molecules within one cell type.

No stable lamellipodium exists for low nucleation rates in figure 4(A), because the creation of new filaments by nucleation cannot compensate for filament extinction by capping and severing. The stable protrusion vanishes for small cross-linking rates $\hat{v}_g^{max}$ since the filaments are long. That entails large severing rates and renders the filaments floppy, which increases the capping rate. Similarly, the filament density decreases with increasing capping rate k_c^{max}

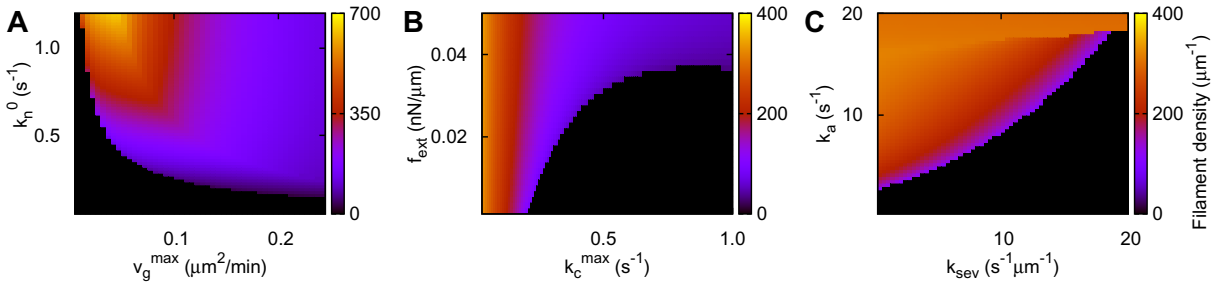

Figure 4. Stationary total filament density: (A) as a function of the cross-linking rate $\hat{v}_g^{max}$ and the nucleation rate k_n^0; (B) as a function of the capping rate k_c^{max} and the external force f_{ext}; (C) as a function of the binding rate of cofilin k_{sev} and attachment rate k_a. There is a bistable domain at large attachment rates. We only show the fixed point with higher filament density. All other parameters are as in table 1.

(figure 4(B)). A larger external force has among others the consequence of decreasing the capping rate via its force dependence (equation (10)). Furthermore, filaments shorten to adapt to the external force, which decreases the severing rate. In this way, applying an external force may cause protrusion formation in the parameter regime shown in figure 4(B). Nucleation is proportional to the number of attached filaments. Consequently, filament binding may cause protrusion generation in figure 4(C).

Besides stable fixed points with a certain filament density, our model also exhibits stable limit cycles. Those limit cycles also correspond to stable lamellipodia. However, the leading edge shows oscillatory motion and varying protrusion velocities. In figure 5, we show two examples of oscillatory solutions of the model. As already discussed in [41], the membrane velocity can either stay at an intermediate value most of the time and periodically drop to lower values during short 'stops' (figure 5(F)), or the membrane periodically jerks forward during short 'jumps' (figure 5(E)). During the phase of slow movement, attached filaments are shorter than z and pull the membrane. The effective cross-linking velocity $\tilde{v}_g$ is larger than the effective polymerization velocity v_p. Consequently, filaments shorten until the force is sufficiently large to disrupt the attached filaments from the membrane and to push it forward. Now the filaments can grow longer again, exert weaker forces and attach to the membrane (see [41] for a detailed description of the oscillation mechanism). The retrograde flow increases or decreases with the membrane velocity since both are proportional to the total filament force. New filaments are nucleated from attached filaments in our model. Due to the nucleation, the total filament density increases when forces are low and the number of attached filaments goes up (figures 5(A) and (B)). The number of capped filaments also increases, because the capping rate is high at low forces, and the filaments are long and it takes longer until they vanish into the gel.

Many mathematical models equate the leading edge velocity with the polymerization rate or a monotonically increasing algebraic function of it. That excludes a phase difference between the maxima of the polymerization rate and leading edge velocity in oscillations. However, such a phase difference has been observed [54]. The leading edge velocity increases first and subsequently the polymerization rate increases. Figure 6 shows the two oscillation types as limit cycles in the phase plane spanned by polymerization velocity v_p and leading edge velocity. The system cycles clockwise in both the cases. The red limit cycle corresponds to oscillations shown

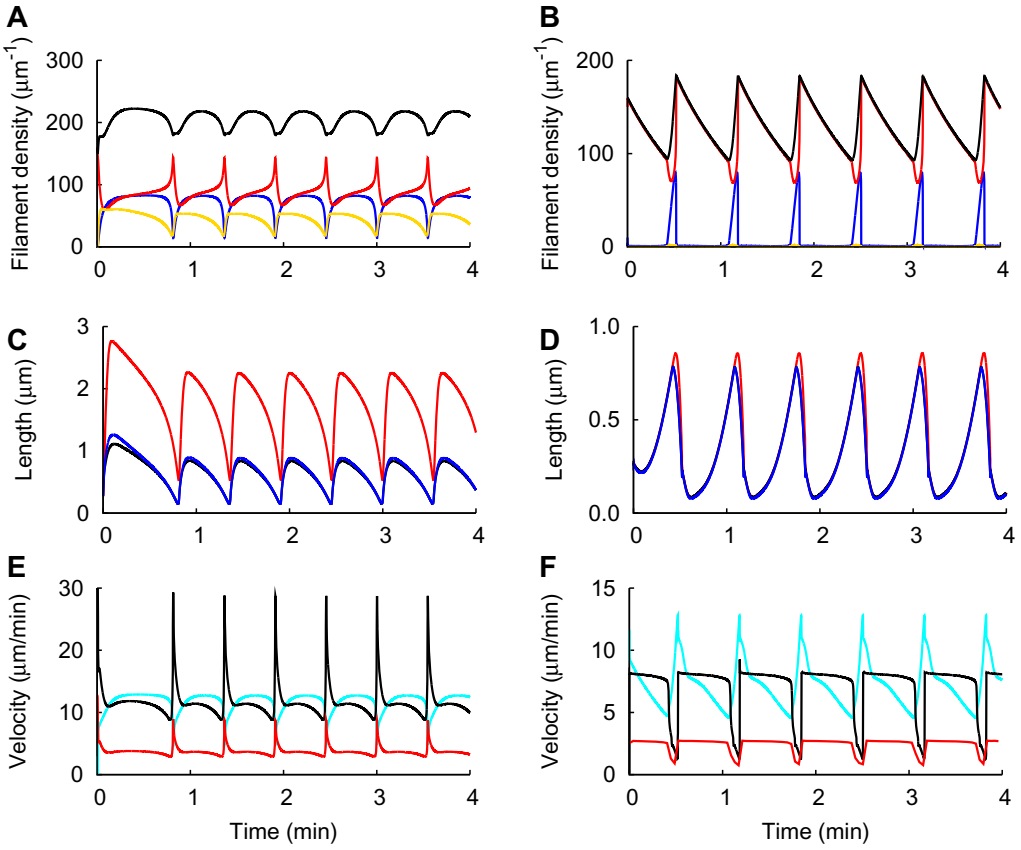

Figure 5. Examples of oscillatory solutions of the model. (A), (B) The density of attached (blue), detached (red) and capped (yellow) filaments and the total filament density (black). (C), (D) The length of the attached (blue) and detached (red) filaments and SR depth (black). (E), (F) Membrane velocity (black), retrograde flow velocity (red) and the velocity of the gel boundary (light blue). (A), (C), (E) For $k_a = 0.2\,s^{-1}$, $k_d^0 = 0.5\,s^{-1}$, $k_c^{max} = 0.23\,s^{-1}$, $v_p^{max} = 78\,\mu m\,min^{-1}$. (B), (D), (F) For $k_a = 0.2\,s^{-1}$, $k_d^0 = 0.3\,s^{-1}$, $k_c^{max} = 0.025\,s^{-1}$, $v_p^{max} = 12\,\mu m\,min^{-1}$. All other parameters are as in table 1.

in figures 5(A), (C) and (E), and the blue one to figures 5(B), (D) and (F)). The phase difference between both velocities in the red limit cycle is obvious. It is about 9 s expressed in time. That is less than the 20 s observed in [54], but we did not search for parameters with longer delays since the important message is the existence of a clear phase difference. The blue limit cycle exhibits almost no phase difference between the two maxima, but the leading edge velocity decreases earlier than the polymerization rate.

In figure 7, we show two examples of bifurcation diagrams where increasing the nucleation rate (figures 7(A), (C) and (E)) or external force (figures 7(B), (D) and (F) leads to a transition from no lamellipodium to a stable, stationarily protruding lamellipodium (a stable fixed point, solid line) to a stable, oscillating lamellipodium (an unstable fixed point, dashed line, a stable limit cycle). In figures 7(A), (C) and (E), the fixed points of the dynamical system are plotted against the nucleation rate k_n^0. At $k_n^0 = 0.25\,s^{-1}$, the nucleation rate becomes large enough to

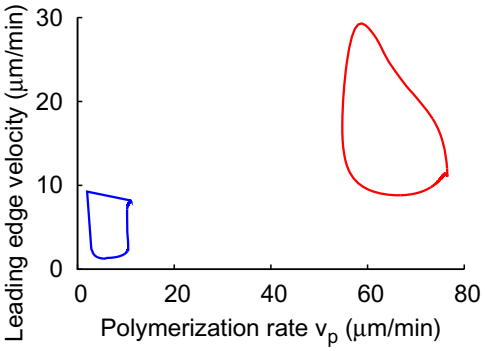

Figure 6. The two oscillation types as limit cycles in the phase plane spanned by polymerization velocity v_p and leading edge velocity. The system cycles clockwise in both the cases. The red limit cycle corresponds to oscillations shown in figures 5(A), (C) and (E), and the blue one to figures 5(B), (D) and (F).

generate a stable fixed point. Attached and detached filaments are both longer than the SR depth z here. The filament density, and therefore also the cross-linking rate, increases with increasing the nucleation rate k_n^0. Consequently, filaments get shorter and exert higher forces. Eventually, attached filaments are shorter than z and the effective cross-linking rate may get larger than the effective polymerization rate, leading to a transition to the oscillatory regime. A stable fixed point different from $n = 0$ can also be generated by increasing the external force (figures 7(B), (D) and (F)). Again, to balance the increasing external force, filaments shorten and their number increases until the fixed point loses stability. Since now the filament density decreases again and the filaments are very short, in the range of the saturation length of the cross-linking velocity, the cross-linking velocity drops below the polymerization velocity and the fixed point becomes stable again upon further growth of force. Note that in those examples attachment rates k_a and detachment rates k_d^0 are lower than in figure 4, which is necessary for observing the oscillations.

3.2. The force–velocity relation

Cells that exhibit stable lamellipodia have to be able to withstand substantial forces from their surroundings. The force–velocity relation describes the lamellipodium protrusion velocity as a function of the force exerted on the leading edge. It is usually measured with a scanning force microscope (SFM) cantilever (see [30]). In [30], we simulated the experimentally measured force–velocity curves with a model with a constant filament density. We now repeat our fit with the model including capping, nucleation and severing. The result is shown in figure 8 and the parameters in table 1. The measured data are still very well reproduced by the model. When the cell touches the cantilever, the velocity of the leading edge drops from $\sim$250 nm s^{-1} to less than 1 nm s^{-1} (figure 8(C)), followed by a concave force–velocity relation (figure 8(B)). As already described in [30], the force–velocity relation mainly gets its characteristic shape due to an initial bending of long filaments and a subsequent adaptation of filament lengths to the increasing external force (figure 8(E)). Retrograde flow slowly increases until it compensates for polymerization in the stalled state (figure 8(C)). The total number of filaments first increases during the concave phase because the capping rate decreases with increasing the force, and severing decreases with shrinking the filament length. Later, the filament number decreases

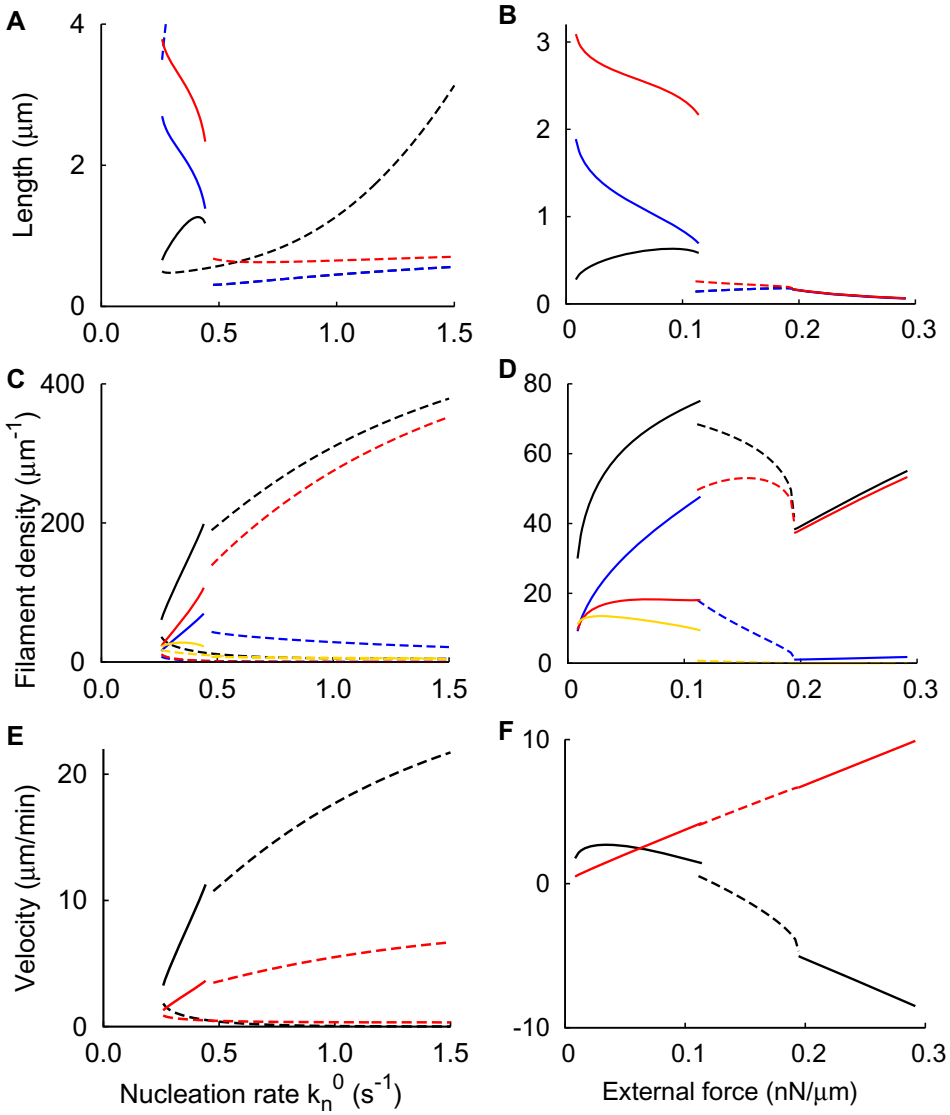

Figure 7. Stationary filament length, SR depth, filament density, membrane and retrograde flow velocity as a function of the nucleation rate k_n^0 (A, C, E) and the external force f_{ext} (B, D, F). (A), (B) The length of attached (blue) and detached (red) filaments and SR depth (black). (C), (D) The density of attached (blue), detached (red) and capped (yellow) filaments and total filament density (black). (E), (F) Membrane (black) and retrograde flow (red) velocity. (Solid lines) A stable fixed point. (Dashed lines) An unstable fixed point; the system oscillates. (A), (C), (E) For $k_a = 0.2\,s^{-1}$ and $k_d^0 = 0.5\,s^{-1}$, $f_{ext} = 0$, all other parameters are as in table 1. The displayed fixed points vanish below $k_n^0 = 0.25\,s^{-1}$. However, there is always another stable fixed point with $n = 0$ and undetermined filament length. Filament lengths larger than 4 µm of the unstable fixed point are not shown in (A). (B), (D), (F)) For $k_a = 0.2\,s^{-1}$, $k_d^0 = 0.5\,s^{-1}$, $k_n^0 = 0.15\,s^{-1}$, $\eta = 4.0\,nN\,s\,\mu m^{-2}$, $\xi = 0.7\,nN\,s\,\mu m^{-3}$, all other parameters are as in table 1. Below $f_{ext} = 0.008\,nN\,\mu m^{-1}$, $n = 0$ is the only stable fixed point. Unlike in (A), (C), (E), we only show the stable fixed point that is then generated and not the unstable fixed point.

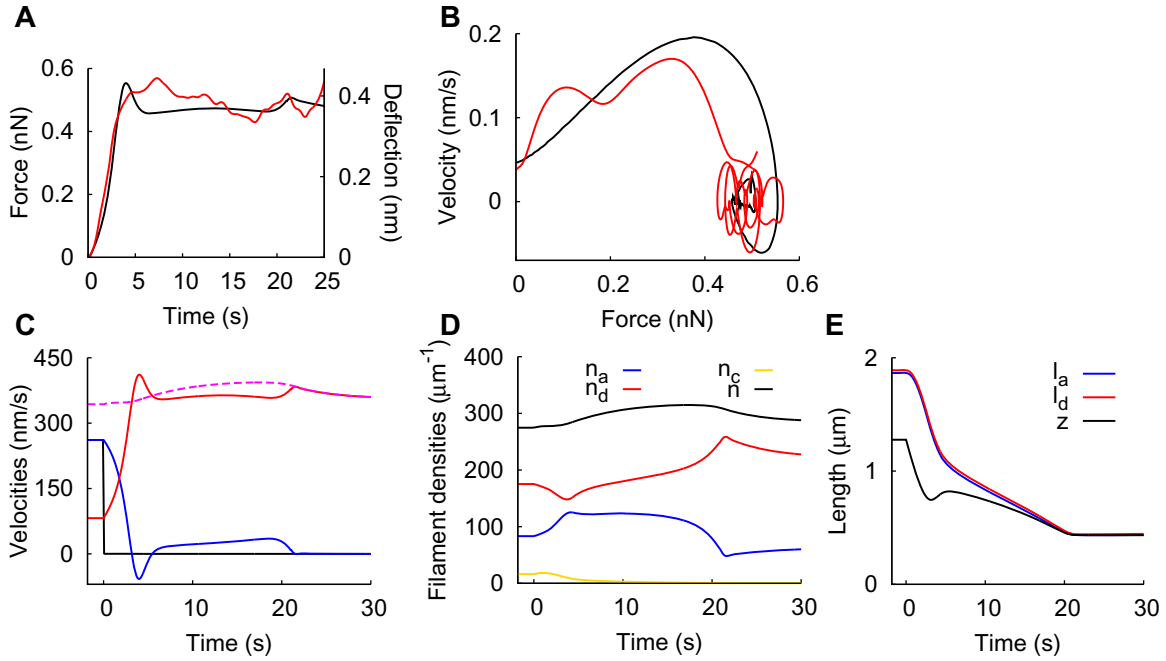

Figure 8. Fit of the experimentally measured dynamic force–velocity relation. (A), (B) Comparison of simulation (black) and experiment (red). (A) Time course of the cantilever deflection, which is proportional to the force exerted on the cell. (B) The force–velocity relation obtained from the deflection and the deflection velocity. (C) Development of the leading edge velocity (black), the gel boundary velocity (blue) and retrograde flow velocity (red). The sum of the latter two (dashed magenta) equals the cross-linking rate and is proportional to the filament density. (D) Time course of filament densities: (blue) attached; (red) detached; (yellow) capped; (black) total. (E) Development of filament lengths ((blue) attached; (red) detached) and the SR depth (black). For the parameter values see table 1.

again, because the ratio of attached to detached filaments decreases and therefore also the nucleation rate. The value in the stalled state is slightly higher than in the freely running cell.

Our model fits the measured protrusion and retrograde flow velocities of the freely running cell before cantilever contact, the velocity measured with the cantilever during the concave phase, the value of the stall force and the shape of the force–velocity relation. Due to the good agreement between the measured data and the simulation, we assume that the model parameters determined by the fit of the force–velocity relation represent the 'default' values for the stable keratocyte lamellipodium in parameter space. We can also conclude some features of the structure of the lamellipodium such as filament length and branch point density. The capping, nucleation and severing rates are relatively low. With the filament density of about $280\,\mu\mathrm{m}^{-1}$ (see figure 8(D)), the effective nucleation rate $k_\mathrm{n} = k_\mathrm{n}^0 - k_\mathrm{n}^N n$ is approximately $9\,\mathrm{min}^{-1}$. Since filaments polymerize in the freely running cell with about $31\mu\mathrm{m\,min}^{-1}$ (the rate of filament elongation equals the rate of filament shortening $n\hat{v}_\mathrm{g}^{\max} l/z$), we should find a branching point approximately every $3.5\,\mu$m along the filament. Filaments in the SR are less than $2\,\mu$m long and consequently the branch point density is low. If we keep in mind that new branches grow from attached filaments only, we find about 50 branch points in the SR per μm lateral width.

Table 1. List of model parameters and their values in figure 8. See also [30].

Symbol	Meaning	Value	Units	Reference
k_a	Attachment rate of filaments to the membrane	10.0	s^{-1}	$10\,s^{-1}$ in [55]
k_d^0	Detachment constant	25.0	s^{-1}	Fitted
v_p^{max}	Saturation value of polymerization velocity	46.2	$\mu m\,min^{-1}$	$30\,\mu m\,min^{-1}$ in [47]
$\hat{v}_g^{max}$	Saturation value of the gel cross-linking rate	0.075	$\mu m^2\,min^{-1}$	Fitted
k_n^0	Nucleation rate	0.6	s^{-1}	[24]
k_n^N	Limiting factor of the nucleation rate	0.0016	$\mu m\,s^{-1}$	Fitted
k_c^{max}	Capping rate	0.065	s^{-1}	[24]
k_{sev}	Binding rate of cofilin	2.0	$s^{-1}\,\mu m^{-1}$	Assumed
$T_{1/2}$	Half-life of ATP-actin within filament	6.0	min	[33]
$\bar{l}$	Saturation length of the cross-linking rate	10		Assumed
κ	Drag coefficient of the plasma membrane	0.113	$nN\,s\,\mu m^{-2}$	[56]
k	Elastic modulus of SFM cantilever	291	$nN\,\mu m^{-2}$	[30]
d	Actin monomer radius	2.7	nm	[57]
l_p	Persistence length of actin	15	μm	[58]
k_l	Spring constant of linker protein	1	$nN\,\mu m^{-1}$	[47, 59]
η	Viscosity of actin gel	0.833	$nN\,s\,\mu m^{-2}$	[60, 61]
ξ	Friction coefficient of actin gel to adhesion sites	0.175	$nN\,s\,\mu m^{-3}$	[62]
μ	Active contractile stress in actin gel	8.33	$pN\,\mu m^{-2}$	Fitted
h_0	Height of lamellipodium at the leading edge	0.25	μm	[63, 64]
L	Length of the gel part of lamellipodium	10	μm	[21, 64]
	Contact length with beads	4.4	μm	[30]

The capping rate is also low. The model result for the density of capped filaments in the freely running cell is approximately $10\,\mu m^{-1}$ (figure 8(D)). We should bear in mind that this is only the number of capped filaments with lengths between z and l_d. Hence, the total number of capped filaments in the SR amounts to $30\,\mu m^{-1}$ (see figure 8(E)). Consequently, to accomplish a stationary filament number, the newly nucleated filaments are partly compensated for by capping, partly by severing. In [24], the authors find on average one branch point every $0.8\,\mu m$ along a filament by evaluating electron microscopy tomograms. However, this value was measured in NIH 3T3 cells and treadmilling is much slower in those cells than in keratocytes, which entails also a smaller branch point distance given a comparable branching rate. The capping and nucleation rates in their simulations ($k_{cap} = 0.03\,s^{-1}$, $k_{br} = 0.042\,s^{-1}$) are slightly lower but in the same range as in our fit (table 1). Moreover, the actual branch point density should be higher because we only account for filament branches that have already grown to the length of the mother filament in our model.

We would like to emphasize that the force–velocity relation measured with the SFM cantilever is not the relation between a constant external force and stationary velocity values. It gets its characteristic shape due to the adaptation of filament length, SR depth and retrograde flow to the increasing external force. The stationary force–velocity relation with the parameter values from our fit of the keratocyte data is shown in figure 9(A). The stationary force–velocity relation is defined as the stationary protrusion velocity at a given constant external force. It is dominated by the force–velocity relation of the gel (equation (14)) and is almost linear. The slight change in slope occurs because the filament density, and therefore also the maximum

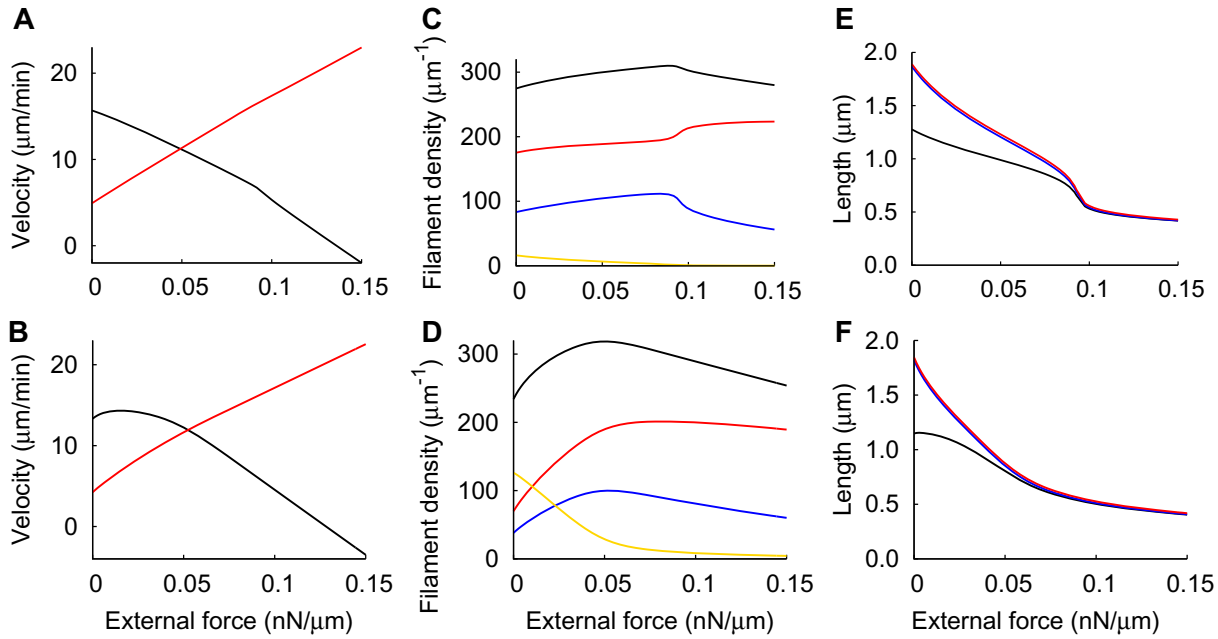

Figure 9. The stationary force–velocity relation and retrograde flow, filament density, filament length and SR depth as a function of the external force. (A), (B) Membrane (black) and retrograde flow (red) velocity. (C), (D) The density of attached (blue), detached (red) and capped (yellow) filaments and total filament density (black). (E), (F) The length of attached (blue) and detached (red) filaments and SR depth (black). (A), (C), (E) For the parameters from the fit of the dynamic force–velocity relation (table 1). (B), (D), (F) For $k_n^0 = 2.2\,s^{-1}$ and $k_c^{max} = 1.0\,s^{-1}$, all other parameters are unchanged.

cross-linking rate, first increases and then decreases (figure 9(C)). Filaments in the SR shorten to balance the increasing external force (figure 9(E)). However, they remain long enough that the effective cross-linking rate does not drop below its maximum value. Otherwise, we could observe a change in slope (see [48]). We find that the stationary force–velocity relation allows for much faster motion for forces below the stall force than the dynamic force–velocity relation. Cells adapt to the constantly applied external force and become faster by that adaptation. It is not possible that a stationary relation exhibits the initial velocity drop seen in the experiment. If we increase the capping and nucleation rates, the maximum in the filament density is more pronounced (figure 9(D)). Consequently, the stationary force–velocity relation has a concave shape (figure 9(B)). The velocity first increases with increasing force, reaches a maximum and then drops. As we see in figures 7(B), (D) and (F), the force–velocity relation can get much more complex for lower attachment and detachment rates. Here, we enter the oscillatory regime by increasing the external force and observe a drop in the stationary velocity.

4. Discussion

Our model provides the conditions for the existence of stable membrane protrusions. The existence of critical values for capping and severing above which stable lamellipodia vanish was

as expected. Here, we assumed that the binding of the capping protein leads to an elongation of the filament by the diameter of this protein. That renders the capping rate force-dependent. While this paper was in press, we indeed learned about experimental results proving the force dependence of the capping rate, which we had used due to thermodynamic considerations, similar to the force dependence of the polymerization rate [65]. Consequently, large forces may reduce the capping rate to a degree sufficient for protrusion formation. Similarly, filaments have to be short to withstand large external forces, which leads to reduced severing. Since we assumed that membrane-bound filaments do not get capped, and new filaments are nucleated from attached filaments, also membrane binding can rescue lamellipodia. The existence of a critical minimal cross-linking rate illustrates that filaments grow too long and floppy for exerting a force and the lamellipodia collapse, if the gelation process does not keep up with leading edge movement. It is important to keep in mind that transient protrusions may exist with less stringent requirements, such as e.g. a difference between gel boundary and leading edge velocity.

The variation of parameters in this study can be interpreted as describing varying states of signaling pathways converging on lamellipodium formation and control or as describing different cell types. The fit of the measured force–velocity relation determines the parameters applying to the stable keratocyte lamellipodium. We can describe other cell types by varying our model parameters. Thus, our model provides an explanation of why some cells exhibit stable, stationarily protruding lamellipodia while others show oscillations of the leading edge or no lamellipodia at all. Different levels of expression or activation of signaling molecules that entail e.g. different nucleation rates lead to the different phenotypes, while the mechanism for lamellipodial protrusion due to actin polymerization is the same in all cells. Our model also suggests which manipulations should lead to the formation of a stable lamellipodium or vice versa its collapse. For example, reducing the nucleation rate in the keratocyte lamellipodium by inhibiting Arp2/3, or reducing the cross-linking rate by inhibiting cross-linking molecules, should lead to a collapse of the lamellipodium. A transition to a lamellipodium exhibiting oscillating protrusion velocities can be achieved by decreasing the attachment and detachment rates of filaments to the membrane.

The response of the cell to external forces depends on the mode of application. Stationary force–velocity relations are shown in figures 7(F) and 9(A), (B). Application of a constant force leads to a piecewise linear force–velocity relation at small filament nucleation rates and can increase the velocity at larger nucleation rates. Force application may also even shift the cell into an oscillatory regime, as in figure 7(F). These examples illustrate that the stationary force–velocity relation does not exhibit a unique shape but may be rather complex. The comparison between figures 8(B), (C) and 9(A) shows the differences between dynamic and stationary force–velocity relations. Hence, our model predicts that the stationary force–velocity relation is different from the dynamic relations measured by force microscopy in [6, 29, 30]. The differences to the dynamic force–velocity relation arise from adaptation to the force by thinning of the SR and a rise in filament density. That a rise in filament density in response to an increasing external force can entail a constant or even increasing velocity has previously been described in the autocatalytic branching model [40] and has been proposed as the mechanism for the force–velocity relation of actin networks [66].

In a realistic lamellipodium, filaments exhibit a variety of lengths and are oriented under different angles [23, 32]. Length distributions of capped filaments were not calculated explicitly in this study because we were mainly interested in the leading edge dynamics, and

short filaments, which cannot exert a force, do not contribute to it. We also do not consider angular distributions. Nevertheless, we are confident that the different regimes found here, no lamellipodia, stable lamellipodia and oscillations, do not depend on this simplification. However, in [67] it was suggested that the filament angular distribution changes under the application of a constant force, and it would be interesting to study whether this influences the stationary force–velocity relation in our model, too. Adhesions are treated as a constant friction between the gel and the substrate in this study. In [30], we have shown that the strengthening of adhesions by the external force does not substantially change the dynamic force–velocity relation. However, further studies are necessary to determine whether remodeling of adhesions contributes to the stationary force–velocity relation.

We have also not included any signaling events in our model. This is certainly a good approximation for the measurement of the dynamic force–velocity relation which takes 5–15 s. Signaling would need to occur even faster. Given, additionally, that the model explains a variety of experimental observations starting with the shape of the complete relation on physical grounds, it seems unlikely that signaling has an essential role in shaping the dynamic force–velocity relation. However, one can imagine that cell signaling, and therefore also our model parameters such as nucleation or polymerization rate, change and adapt if a stationary force is applied to the lamellipodium. Our simulations of the stationary force–velocity relation allow determining whether signaling has a role there by comparing our results with future experiments. Moreover, it is interesting to note that signaling is not necessary for the adaptation of the filament density to the force.

References

[1] Bray D 2001 *Cell Movements—From Molecules to Motility* 2nd edn (New York: Garland)
[2] Wedlich D (ed) 2004 *Cell Migration in Development and Disease* (New York: Wiley-VCH)
[3] Friedel P, Hegerfeld Y and Tusch M 2004 Collective cell migration in morphogenesis and cancer *Int. J. Dev. Biol.* **48** 441–9
[4] Zhong J, Paul A, Kellie S J and Neill G M 2010 Mesenchymal migration as a therapeutic target in glioblastoma *J. Oncol.* **2010** 430142
[5] Marcy Y, Prost J, Carlier M-F and Sykes C 2004 Forces generated during actin-based propulsion: a direct measurement by micromanipulation *Proc. Natl Acad. Sci. USA* **101** 5992–7
[6] Prass M, Jacobson K, Mogilner A and Radmacher M 2006 Direct measurement of the lamellipodial protrusive force in a migrating cell *J. Cell Biol.* **174** 767–72
[7] Pollard T D 2003 The cytoskeleton, cellular motility and the reductionist agenda *Nature* **422** 741–5
[8] Ichetovkin I, Grant W and Condeelis J 2002 Cofilin produces newly polymerized actin filaments that are preferred for dendritic nucleation by the Arp2/3 complex *Curr. Biol.* **12** 79–84
[9] Ghosh M, Song X, Mouneimne G, Sidani M, Lawrence D S and Condeelis J S 2004 Cofilin promotes actin polymerization and defines the direction of cell motility *Science* **304** 743–6
[10] Stradal T E B, Rottner K, Disanza A, Confalonieri S, Innocenti M and Scita G 2004 Regulation of actin dynamics by wasp and wave family proteins *Trends Cell Biol.* **14** 303–11
[11] Carlier M-F and Pantaloni D 2007 Control of actin assembly dynamics in cell motility *J. Biol. Chem.* **282** 23005–9
[12] Delorme V, Machacek M, DerMardirossian C, Anderson K L, Wittmann T, Hanein D, Waterman-Storer C, Danuser G and Bokoch G M 2007 Cofilin activity downstream of Pak1 regulates cell protrusion efficiency by organizing lamellipodium and lamella actin networks *Dev. Cell* **13** 646–62

[13] Le Clainche C and Carlier M-F 2008 Regulation of actin assembly associated with protrusion and adhesion in cell migration *Physiol. Rev.* **88** 489–513
[14] Enculescu M and Falcke M 2012 Modeling morphodynamic phenotypes and dynamic regimes of cell motion *Advances in Experimental Medicine and Biology* vol 736 (Berlin: Springer) chapter 20 pp 337–58
[15] Verkhovsky A B, Svitkina T M and Borisy G G 1999 Self-polarization and directional motility of cytoplasm *Curr. Biol.* **9** 11–20
[16] Lenz P, Keren K and Theriot J A 2008 Biophysical aspects of actin-based cell motility in fish epithelial keratocytes *Cell Motility, Biological and Medical Physics, Biomedical Engineering* (New York: Springer) pp 31–58
[17] Timpson P and Daly R J 2005 Distinction at the leading edge of the cell *Bioessays* **27** 349–52
[18] Small J V and Resch G P 2005 The comings and goings of actin: coupling protrusion and retraction in cell motility *Curr. Opin. Cell Biol.* **17** 517–23
[19] Small J V, Auinger S, Nemethova M, Koestler S, Goldie K N, Hoenger A and Resch G P 2008 Unravelling the structure of the lamellipodium *J. Microsc.* **231** 479–85
[20] Vallotton P and Small J V 2009 Shifting views on the leading role of the lamellipodium in cell migration: speckle tracking revisited *J. Cell Sci.* **122** 1955–8
[21] Svitkina T M, Verkhovsky A B, McQuade K M and Borisy G G 1997 Analysis of the actin–myosin II system in fish epidermal keratocytes: mechanism of cell body translocation *J. Cell Biol.* **139** 397–415
[22] Verkhovsky A B, Oleg Y Chaga, Sebastien Schaub, Tatyana M Svitkina, Meister J-J and Borisy G G 2003 Orientational order of the lamellipodial actin network as demonstrated in living motile cells *Mol. Biol. Cell* **14** 4667–75
[23] Urban E, Jacob S, Nemethova M, Resch G P and Small J V 2010 Electron tomography reveals unbranched networks of actin filaments in lamellipodia *Nature Cell Biol.* **12** 429–35
[24] Vinzenz M *et al* 2012 Actin branching in the initiation and maintenance of lamellipodia *J. Cell Sci.* **125** 2775–85
[25] Yang C and Svitkina T 2011 Visualizing branched actin filaments in lamellipodia by electron tomography *Nature Cell Biol.* **13** 1012–3
[26] Small J V, Winkler C, Vinzenz M and Schmeiser C 2011 Reply: visualizing branched actin filaments in lamellipodia by electron tomography *Nature Cell Biol.* **13** 1013–4
[27] Gardel M L, Shin J H, MacKintosh F C, Mahadevan L, Matsudaira P and Weitz D A 2004 Elastic behavior of cross-linked and bundled actin networks *Science* **304** 1301–5
[28] Bohnet S, Ananthakrishnan R, Mogilner A, Meister J-J and Alexander B Verkhovsky 2006 Weak force stalls protrusion at the leading edge of the lamellipodium *Biophys. J.* **90** 1810–20
[29] Heinemann F, Doschke H and Radmacher M 2011 Keratocyte lamellipodial protrusion is characterized by a concave force–velocity relation *Biophys. J.* **100** 1420–7
[30] Zimmermann J, Brunner C, Enculescu M, Goegler M, Ehrlicher A, Käs J and Falcke M 2012 Actin filament elasticity and retrograde flow shape the force–velocity relation of motile cells *Biophys. J.* **102** 287–95
[31] Small J V, Herzog M and Anderson K 1995 Actin filament organization in the fish keratocyte lamellipodium *J. Cell Biol.* **129** 1275–86
[32] Koestler S A, Auinger S, Vinzenz M, Rottner K and Small J V 2008 Differentially oriented populations of actin filaments generated in lamellipodia collaborate in pushing and pausing at the cell front *Nature Cell Biol.* **10** 306–13
[33] Pollard T D and Borisy G G 2003 Cellular motility driven by assembly and disassembly of actin filaments *Cell* **112** 453–65
[34] Trichet L, Campas O, Sykes C and Plastino J 2007 VASP governs actin dynamics by modulating filament anchoring *Biophys. J.* **92** 1081–9
[35] Sheetz M P and Dai J 1996 Modulation of membrane dynamics and cell motility by membrane tension *Trends Cell Biol.* **6** 85–9
[36] Keren K 2011 Membrane tension leads the way *Proc. Natl Acad. Sci. USA* **108** 14379–80

[37] Liu Y *et al* 2012 Constitutively active ezrin increases membrane tension, slows migration and impedes endothelial transmigration of lymphocytes in vivo in mice *Blood* **119** 445–53
[38] Houk A R, Jilkine A, Mejean C O, Boltyanskiy R, Dufresne E R, Angenent S B, Altschuler S J, Wu L F and Weiner O D 2012 Membrane tension maintains cell polarity by confining signals to the leading edge during neutrophil migration *Cell* **148** 175–88
[39] Enculescu M, Sabouri-Ghomi M, Danuser G and Falcke M 2010 Modeling of protrusion phenotypes driven by the actin-membrane interaction *Biophys. J.* **98** 1571–81
[40] Carlsson A E 2003 Growth velocities of branched actin networks *Biophys. J.* **84** 2907–18
[41] Enculescu M, Gholami A and Falcke M 2008 Dynamic regimes and bifurcations in a model of actin-based motility *Phys. Rev.* E **78** 031915
[42] Faber M, Enculescu M and Falcke M 2010 Filament capping and nucleation in actin-based motility *Eur. Phys. J. Spec. Top.* **191** 147–58
[43] Gholami A, Wilhelm J and Frey E 2006 Entropic forces generated by grafted semiflexible polymers *Phys. Rev.* E **74** 041803
[44] Gholami A, Falcke M and Frey E 2008 Velocity oscillations in actin-based motility *New J. Phys.* **10** 033022
[45] Kroy K and Frey E 1996 Force-extension relation and plateau modulus for wormlike chains *Phys. Rev. Lett.* **77** 306–9
[46] Kroy K 1998 *Viskoelastizität von Lösungen Halbsteifer Polymere* (München: Hieronymus)
[47] Mogilner A and Oster G 2003 Force generation by actin polymerization: ii. The elastic ratchet and tethered filaments *Biophys. J.* **84** 1591–605
[48] Zimmermann J, Enculescu M and Falcke M 2010 Leading-edge–gel coupling in lamellipodium motion *Phys. Rev.* E **82** 051925
[49] Carlier M-F, Laurent V, Santolini J, Melki R, Didry D, Xia G-X, Hong Y, Chua N-H and Pantaloni D 1997 Actin depolymerizing factor (ADF/Cofilin) enhances the rate of filament turnover: implication in actin-based motility *J. Cell Biol.* **136** 1307–22
[50] Blanchoin L and Pollard T D 1998 Interaction of actin monomers with acanthamoeba actophorin (ADF/cofilin) and profilin *J. Biol. Chem.* **273** 25106–11
[51] Kruse K, Joanny J F, Jülicher F, Prost J and Sekimoto K 2005 Generic theory of active polar gels: a paradigm for cytoskeletal dynamics *Eur. Phys. J.* E **16** 5–16
[52] Kruse K, Joanny J F, Jülicher F and Prost J 2006 Contractility and retrograde flow in lamellipodium motion *Phys. Biol.* **3** 130–7
[53] Zajac M, Dacanay B, Mohler W A and Wolgemuth C W 2008 Depolymerization-driven flow in nematode spermatozoa relates crawling speed to size and shape *Biophys. J.* **94** 3810–23
[54] Ji L, Lim J and Danuser G 2008 Fluctuations of intracellular forces during cell protrusion *Nature Cell Biol.* **10** 1393–400
[55] Shaevitz J W and Fletcher D A 2007 Load fluctuations drive actin network growth *Proc. Natl Acad. Sci. USA* **104** 15688–92
[56] Berg H 1983 *Random Walks in Biology* (Princeton, NJ: Princeton University Press)
[57] Mogilner A 2009 Mathematics of cell motility: have we got its number? *J. Math. Biol.* **58** 105–34
[58] Le Goff L, Hallatschek O, Frey E and Amblard F 2002 Tracer studies on f-actin fluctuations *Phys. Rev. Lett.* **89** 258101
[59] Evans E 2001 Probing the relation between force and chemistry in single molecular bonds *Annu. Rev. Biophys. Biomol. Struct.* **30** 105–28
[60] Bausch A R, Ziemann F, Boulbitch A A, Jacobson K and Sackmann E 1998 Local measurements of viscoelastic parameters of adherent cell surfaces by magnetic bead microrheometry *Biophys. J.* **75** 2038–49
[61] Yanai M, Butler J P, Suzuki T, Sasaki H and Higuchi H 2004 Regional rheological differences in locomoting neutrophils *Am. J. Physiol. Cell Physiol.* **287** C603–11
[62] Doyle A, Marganski W and Lee J 2004 Calcium transients induce spatially coordinated increases in traction force during the movement of fish keratocytes *J. Cell Sci.* **117** 2203–14

[63] Anderson K I, Wang Y L and Small J V 1996 Coordination of protrusion and translocation of the keratocyte involves rolling of the cell body *J. Cell Biol.* **134** 1209–18

[64] Brunner C, Ehrlicher A, Kohlstrunk B, Knebel D, Käs J and Goegler M 2006 Cell migration through small gaps *Eur. Biophys. J.* **35** 713–9

[65] Bieling P, Li T-D, Mullins R D and Fletcher D A 2012 The mechanobiochemistry of dendritic actin network assembly *Talk at the Annual Meeting of the American Society for Cell Biology* (*San Francisco, CA, 15–19 December*)

[66] Parekh S H, Chaudhuri O, Theriot J A and Fletcher D A 2005 Loading history determines the velocity of actin-network growth *Nature Cell Biol.* **7** 1219–23

[67] Weichsel J and Schwarz U S 2010 Two competing orientation patterns explain experimentally observed anomalies in growing actin networks *Proc. Natl Acad. Sci. USA* **107** 6304–9